# New quantum numbers in collision theory. II. Angular momentum diagrams and interpretation

Chun-Woo Lee
*James Franck Institute, University of Chicago, 5640 South Ellis Avenue, Chicago, Illinois 60637*
(Received 24 March 1986)

Geometrical relationships illustrate the significance of the transformation between new and orbital quantum numbers. The semiclassical analysis of $6j$ coefficients by Ponzano and Regge clarifies the geometrical relationships and identifies a classically forbidden range, which can be singled out for its small contribution to the summation over the partial waves relevant to observable parameters (differential cross section and orientation).

## I. INTRODUCTION

The analysis of light emitted or absorbed by atoms or molecules in collision processes has provided important data on their polarization and also on their internal dynamics, for example, through the observation of quantum beats.[1] This success rests largely on the circumstance that light exchanges usually just one unit of angular momentum with matter. On the other hand, general collision processes involve orbital motions with high angular momenta which complicate greatly the extraction of the significant parameters from experimental data.

Collision theory might nevertheless be restructured more nearly along lines analogous to the analysis of photoprocesses. It is helpful to this end to identify and simplify the role of high orbital momenta in the theory. Note in this connection that standard theory[2] involves as many as four orbital momenta $\{l_a,l_b,l'_a,l'_b\}$, each of which runs from 0 to $\infty$. An alternative set of quantum numbers $\{\sigma,\tau,\zeta,\eta\}$ has been introduced recently[3] to replace the $l$'s. Among these only $\sigma$ runs to $\infty$. In the special case of the process[4]

$$e+\mathrm{He}(1^1S)\rightarrow e'+\mathrm{He}(n\,^1P) \tag{1}$$

treated in Ref. 3, only four combinations of $(\zeta,\eta)$ occur, namely $(0,\pm1)$ and $(\pm1,0)$, because the angular momentum transferred to the target is restricted to $j_t=1$.

The theoretical cross section and target orientation of process (1) were resolved by Ref. 3 into two components, with $\zeta=0$ or $\eta=0$, upon introduction of $\{\sigma,\tau,\zeta,\eta\}$. Their dynamical parameters are then grouped hierarchically, first according to their values of $\eta$ (or $\zeta$), then according to $\tau$ and finally according to $\sigma$. Fuller interpretation and application of the new quantum numbers were seen in Ref. 3 to require much further elaboration.

Section II of this paper illustrates the above hierarchical structure by analyzing the geometry of the tetrahedron composed of the vector angular momenta $\{l_a,l_b,l'_a,l'_b\}$ and of their differences (with * added according to Schwinger[5])

$$\mathbf{k}=l'_a-l^*_a=l'_b-l^*_b\ , \tag{2}$$

$$\mathbf{j}_t=l_b-l^*_a=l'_b-l'^*_a\ . \tag{3}$$

This illustration may appear semiclassical, but Ponzano and Regge[6,7] showed that including a phase term in semiclassical treatments yields very good approximations even for small angular momenta. The vertices of this tetrahedron lie on conic sections with parameters $\{\sigma,\tau,\zeta,\eta\}$. The tetrahedron may then be studied through its dependence on the conic sections (roughly speaking, on its size and distortion) rather than on the length of each of its edges. The geometrical relationships between the orbital and the new quantum numbers also illustrate the contrast between the alternative cases $\zeta=0$ and $\eta=0$. Consideration of large and small $\sigma$ values reveals that the construction of the tetrahedron is not always possible, with implications previously discussed by Ponzano and Regge.

Section III will then utilize the work of Ponzano and Regge, a semiclassical theory of $6j$ coefficients, showing how a tetrahedron cannot be constructed when the indices of a $6j$ coefficient are in a "classically forbidden" range. The values of $6j$ coefficients are oscillating functions in the allowed range and decay exponentially beyond its boundaries. Accordingly, a part of the summation ranges in the cross section and orientation formulas is singled out by its small contribution. The implication of this result for the mechanism of orientation will be treated in a later paper.

## II. GEOMETRICAL RELATION OF SYMMETRICAL AND ORBITAL QUANTUM NUMBERS

A set of symmetrical quantum numbers was defined in Ref. 3 as

$$\begin{aligned}\sigma&=\tfrac{1}{2}(l_a+l_b+l'_a+l'_b)\ ,\\ \tau&=\tfrac{1}{2}(l_a+l_b-l'_a-l'_b)\ ,\\ \zeta&=\tfrac{1}{2}(l_a-l_b+l'_a-l'_b)\ ,\\ \eta&=\tfrac{1}{2}(l_a-l_b-l'_a+l'_b)\ ,\end{aligned} \tag{4}$$

where the $l$'s denote the projectile electron's orbital momenta in the system (1); $a$ and $b$ stand for the initial and final states and the prime stands for the complex conjugate state of the unprimed state.

 

The replacement of $l$ by $l+\frac{1}{2}$, familiar in semiclassical treatments, leads to replacing $\sigma$ by $\bar{\sigma}=\sigma+1$ without changing the other quantum numbers $(\tau,\zeta,\eta)$. By a simple transformation of Eq. (4), we thus get

$$\begin{aligned}\bar{\sigma}+\zeta&=(l_a+\tfrac{1}{2})+(l'_a+\tfrac{1}{2})\,,\\ \tau+\eta&=(l_a+\tfrac{1}{2})-(l'_a+\tfrac{1}{2})\,,\end{aligned}\tag{5}$$

and

$$\begin{aligned}\bar{\sigma}-\zeta&=(l_b+\tfrac{1}{2})+(l'_b+\tfrac{1}{2})\,,\\ \tau-\eta&=(l_b+\tfrac{1}{2})-(l'_b+\tfrac{1}{2})\,.\end{aligned}\tag{6}$$

In (5) $l_a+\frac{1}{2}$ and $l'_a+\frac{1}{2}$ represent the lengths of vectors $l_a$ and $l'_a$, respectively, which form a triangle with $\mathbf{k}$ by the vector equation (2). If we vary $l_a$ and $l'_a$ in this triangle keeping $\mathbf{k}$ fixed such that the first (5) be satisfied, the locus of the point $P$ in Fig. 1 will be the ellipse with the (major) axis $\bar{\sigma}+\zeta$ and with foci $FF'$ at the distance $k+\frac{1}{2}$. The second (5) similarly requires $l_a$ and $l'_a$ to terminate at a point $Q$ on the hyperbola with (transverse) axis $\tau+\eta$. The points $A$, intersections of the loci $P$ and $Q$, represent positions that fulfill both equations (5). The same construction, with axes $\bar{\sigma}-\zeta$ and $\tau-\eta$, identify the intersections $B$ that fulfil the conditions (6) on $l_b$ and $l'_b$.

The separate constructions based on (5) and (6) can now be combined in Fig. 2, where two half planes $a$ and $b$ share the vector $\mathbf{k}$ on their common edge. The angle between the half planes is fixed by requiring the distance $AB$ to equal $j_t+\frac{1}{2}$ in accordance with (3). The four points $\{F,F',A,B\}$ form the vertices of a tetrahedron which represents the six vectors $\{l_a,l_b,l'_a,l'_b,\mathbf{k},\mathbf{j}_t\}$. However, the tetrahedron could not be constructed if $j_t+\frac{1}{2}$ were shorter than the distance $AB$ when the half planes $a$ and $b$ coincide, or longer than $AB$ when their angle reaches 180°.

The restrictions on the eccentricities of the conic sections imply the previous result in Ref. 3 on the allowed ranges of the symmetrical quantum numbers

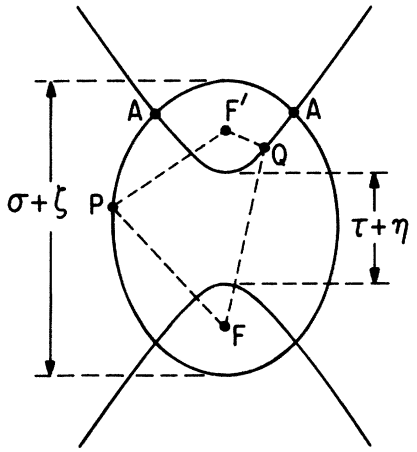


FIG. 1. Ellipse and hyperbola in the plane $a$. $\mathbf{F}-\mathbf{F}'=\mathbf{k}$, $\mathbf{F}-\mathbf{P}=l_a$, $\mathbf{F}-\mathbf{P}=l'_a$; the vector lengths are $k+\frac{1}{2}$, $l_a+\frac{1}{2}$, and $l'_a+\frac{1}{2}$, respectively.

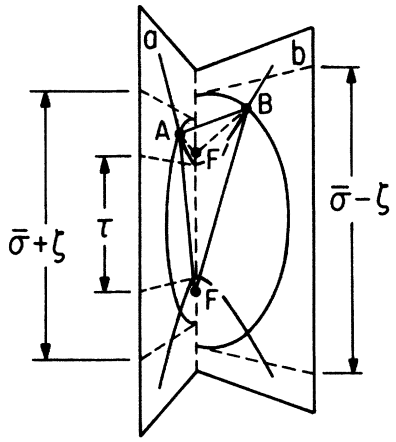


FIG. 2. Tetrahedron, ellipse, and hyperbola in the planes $a$ and $b$. $\mathbf{F}-\mathbf{F}'=\mathbf{k}$, $\mathbf{A}-\mathbf{F}=l'_a$, $\mathbf{A}-\mathbf{F}=l_a$, $\mathbf{B}-\mathbf{F}'=l'_b$, $\mathbf{B}-\mathbf{F}=l_b$, $\mathbf{A}-\mathbf{B}=\mathbf{j}_t$; vector lengths are $k+\frac{1}{2}$, $l'_a+\frac{1}{2}$, $l_a+\frac{1}{2}$, $l'_b+\frac{1}{2}$, $l_b+\frac{1}{2}$, and $j_t+\frac{1}{2}$, respectively.

$$\bar{\sigma}\geq k+|\zeta|+\tfrac{1}{2},\quad \tau\leq k-|\eta|+\tfrac{1}{2}\,.\tag{7}$$

The operation $P(l_a,l_b)=(l'_a,l'_b)$ of Ref. 3, corresponding to $P(\tau,\eta)=(-\tau,-\eta)$ shifts the points $A$ and $B$ from the upper branches of the hyperbolas in Fig. 2 to their lower branches. The operators $Q(l_a,l'_a)=(l_b,l'_b)$, corresponding to $Q(\zeta,\eta)=(-\zeta-\eta)$, changes the dihedral angle between planes $a$ and $b$ from $\theta$ to $\pi-\theta$.

The restriction $j_t=1$ on the collision (1) restricts the values of $(\zeta,\eta)$ to the alternative pairs $(0,\pm1)$ and $(\pm1,0)$. For $\eta=0$ Fig. 2 shows ellipses with two major axes $\bar{\sigma}\pm1$ but hyperbolas with the single transverse axis $\tau$; for $\zeta=0$ $(\eta\neq0)$ it would show hyperbolas with two axes $\tau\pm1$ but ellipses with a single axis $\bar{\sigma}$. Note that the pairs of points $(A,B)$ lie generally on the same branch of a hyperbola with the following exceptions: (1) $\zeta=0$, $\tau=0$; (2) $\zeta=0$, $\tau=\pm1$, in which case the hyperbola in one of the two half planes collapses into a single straight line orthogonal to $\mathbf{k}$; (3) $\eta=0,\tau=0$ in which case both hyperbolas collapse into a line and both $\mathbf{A}$ and $\mathbf{B}$ are equidistant from $\mathbf{F}$ and $\mathbf{F}'$.

### A. Large values of $\bar{\sigma}$

In the limit of very large orbital numbers, $\bar{\sigma}\to\infty$, the ellipses become circles with radius $\bar{\sigma}/2$ and their intersections $\mathbf{A}$ and $\mathbf{B}$ lie on the asymptotes of the hyperbola with slopes $\pm\{[(k+1/2)/\tau]^2-1\}^{1/2}$. In this event no effective restriction to the construction of the tetrahedron occurs for $\eta=0$. The minimum of the length $|\mathbf{A}-\mathbf{B}|$ equals unity and its maximum equals $\bar{\sigma}\{1-[\tau/(k+\frac{1}{2})]^2\}^{1/2}=O(\bar{\sigma})$; therefore the actual length $|\mathbf{A}-\mathbf{B}|$, $j_t+\frac{1}{2}=1.5$, lies between the maximum and minimum of the lengths $|\mathbf{A}-\mathbf{B}|$ and the tetrahedron can be constructed. For $\zeta=0$ $(\eta\neq0)$, on the contrary, even the minimum of the length $|\mathbf{A}-\mathbf{B}|$ becomes of $O(\bar{\sigma})$ as seen in Fig. 3 and the construction of the tetrahedron is generally impossible within the realm of the ordinary geometry [the projective geometry called PG$(n,2)$ would remove this barrier[6]].

Let us now examine in greater detail when it is possible

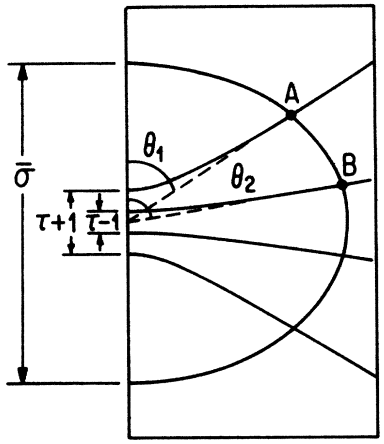


FIG. 3. $\zeta=0$, with coincident planes $a$ and $b$. The arc length of $|\mathbf{A}-\mathbf{B}|$ is approximately given by $(\theta_2-\theta_1)\bar{\sigma}/2$.

to construct the tetrahedron, beginning with the $\tau=0$ ($\zeta=0$) case. The length $|\mathbf{A}-\mathbf{B}|$ is given here by $\bar{\sigma}/(k+\frac{1}{2})$ ($\bar{\sigma}=k+1,k+3,\ldots$), which already exceeds $j_t+\frac{1}{2}$ for $\bar{\sigma}=3$ ($k=1$) or $\bar{\sigma}=4$ ($k=2$). In this case the tetrahedron can be constructed only for $\bar{\sigma}=2$ ($k=1$) and for $\bar{\sigma}=3$ ($k=2$); on the other hand, more values of $\bar{\sigma}$ are allowed for the construction of the tetrahedron at large $k$, e.g., five values of $\bar{\sigma}$, i.e., 21, 23, 25, 27, and 29 are allowed for $k=20$ (this argument is actually independent of the values of $\tau$ as discussed in Appendix A). For the process (1) at impact energy $\leq 80$ eV, values of $k$ larger than 20 give a negligible contribution to measurable quantities; for $\zeta=0$, therefore, no tetrahedron can be constructed for most significant values of $\bar{\sigma}$.

### B. Small values of $\bar{\sigma}$

We saw in Sec. II A that the construction of the tetrahedron can only be possible for the first few smallest values of $\bar{\sigma}$ when $\zeta=0$ but is always possible for large values of $\bar{\sigma}$ when $\eta=0$. Figure 4 shows that a different

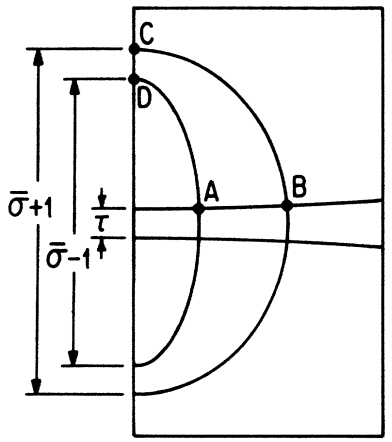


FIG. 4. $\eta=0$ ($\bar{\sigma}=9$, $k=7$, $\tau=1$), with coincident planes $a$ and $b$. The length $|\mathbf{C}-\mathbf{D}|$ is given by 1, smaller than $j_t+\frac{1}{2}$, but the length $|\mathbf{A}-\mathbf{B}|$ is larger than $j_t+\frac{1}{2}$.

limit to the construction of the tetrahedron operates for small values of $\bar{\sigma}$ when $\eta=0$. The minimum distance $|\mathbf{A}-\mathbf{B}|$ exceeds $j_t+\frac{1}{2}$ for small values of $\bar{\sigma}$ when $\eta=0$ (and small $\tau$) owing to the rapid growth of the ellipse in the neighborhood of the minor axis as $\bar{\sigma}$ increases. When $\eta=0$ and $\tau=0$, the minimum distance $|\mathbf{A}-\mathbf{B}|$ is given by $\frac{1}{2}\{[(\bar{\sigma}+1)^2-(k+1/2)^2]^{1/2}-[(\bar{\sigma}-1)^2-(k+\frac{1}{2})^2]^{1/2}\}$ and exceeds $j_t+\frac{1}{2}$ for the single value of $\bar{\sigma}=k+2$ when $10>k\geq 4$, and for two values of $\bar{\sigma}=k+2$, $k+4$ when $16>k\geq 10$. Thus no tetrahedron can be constructed for the first one or two values of $\bar{\sigma}$ when $\eta=0$ and $\tau=0$ for a small but physically important range of $k$. This occurrence becomes rare for large $|\tau|$ and the tetrahedron can be constructed for all values of $\bar{\sigma}$ for $\tau=k$.

In summary, when $\eta=0$, the tetrahedron can be constructed for most values of $\bar{\sigma}$, the more so as $|\tau|$ becomes large. When $\zeta=0$, instead, the tetrahedron cannot be constructed for most values of $\bar{\sigma}$ regardless of $\tau$, except for the first few ones.

Besides the confocal system of conic sections described above, two other systems of conic sections may be constructed starting from linear combinations of (5) and (6), yielding $\bar{\sigma}\pm\tau$ or $\bar{\sigma}\pm\eta$ instead of $\bar{\sigma}\pm\zeta$. The first of these yields confocal conic sections with focal distance $j_t+\frac{1}{2}$, but fails to utilize the expansion of observables into Legendre polynomials $P_{kq}(\cos\theta)$. The other one is even less convenient because it does not lead to a confocal system.

### C. The meaning of $\zeta$ and $\eta$

In the confocal coordinate system of prolate spheroids and hyperboloids with focal distance $k+\frac{1}{2}$ implied by the full three-dimensional version of Fig. 2, let us consider the pair of points $(A,B)$ in Fig. 2 separated by $|\zeta|$ and $|\eta|$ from the reference point with coordinate $(\bar{\sigma},\tau,\phi)$. These two points $(\bar{\sigma}+\zeta,\tau+\eta,\phi_1)$ and $(\bar{\sigma}-\zeta,\tau-\eta,\phi_2)$ together with the focal points (**FF'**) compose the tetrahedron considered above, when $\phi_1$ and $\phi_2$ are chosen so that the distance between our two points is $j_t+\frac{1}{2}$. The magnitudes $|\zeta|$ and $|\eta|$ thus denote the allowed range of variation of $\mathbf{j}_t$ for fixed values of $\bar{\sigma}$ and $\tau$, respectively. The tetrahedron cannot be constructed if this constraint on $\mathbf{j}_t$ excludes its actual magnitude $j_t+\frac{1}{2}$. The rigidity of this constraint is measured by the sensitivity of the distance $|\mathbf{A}-\mathbf{B}|$ to variations of $\zeta$ and $\eta$, that is, by the pair of parameters

$$h_{\bar{\sigma}}\equiv\left[\frac{\partial|\mathbf{A}-\mathbf{B}|}{\partial\zeta}\right]_{\eta=0}=\left[\frac{\bar{\sigma}^2-\tau^2}{\bar{\sigma}^2-(k+\frac{1}{2})^2}\right]^{1/2},$$
$$h_{\tau}\equiv\left[\frac{\partial|\mathbf{A}-\mathbf{B}|}{\partial\eta}\right]_{\zeta=0}=\left[\frac{\bar{\sigma}^2-\tau^2}{(k+\frac{1}{2})^2-\tau^2}\right]^{1/2}. \tag{8}$$

The limiting values of these parameters, as $\bar{\sigma}$ rises from its minimum $k+\frac{1}{2}$ to $\infty$, are

$$h_{\bar{\sigma}}\rightarrow\begin{cases}1 & \text{as } \bar{\sigma}\rightarrow\infty\\ \infty & \text{as } \bar{\sigma}\rightarrow k+\frac{1}{2}\end{cases},\qquad h_{\tau}\rightarrow\begin{cases}\infty & \text{as } \bar{\sigma}\rightarrow\infty\\ 1 & \text{as } \bar{\sigma}\rightarrow k+\frac{1}{2}\end{cases}, \tag{9}$$

showing the same structures as in Secs. II A and II B.

## III. PONZANO AND REGGE'S SEMICLASSICAL EXTENSION OF THE VECTOR MODEL

We have seen in Sec. II that the construction of ellipses and hyperbolas in Fig. 2 need not allow the formation of a tetrahedron, depending on the magnitudes of the angular momentum vectors. An algebraic treatment of this problem has been done by Ponzano and Regge[6,7] in terms of the volume of the tetrahedron as a function of the indices of a $6j$ coefficient. The square of this volume is represented by the Cayley determinant (p. 380 of Ref. 7)

$$288\,V^2=\det\begin{bmatrix}0 & j_{34}^2 & j_{24}^2 & j_{23}^2 & 1\\ j_{34}^2 & 0 & j_{14}^2 & j_{13}^2 & 1\\ j_{24}^2 & j_{14}^2 & 0 & j_{12}^2 & 1\\ j_{23}^2 & j_{13}^2 & j_{12}^2 & 0 & 1\\ 1 & 1 & 1 & 1 & 0\end{bmatrix}, \tag{10}$$

where $\{j_{13},j_{14},j_{24},j_{23},j_{12},j_{34}\}$ denote $\{l_a+\frac{1}{2},l_b+\frac{1}{2},l'_a+\frac{1}{2},l'_b+\frac{1}{2},j_t+\frac{1}{2},k+\frac{1}{2}\}$, respectively. Ponzano and Regge pointed out then that values of $j_{hk}$ compatible with the triangular conditions may yield a negative value of (10), for which no real tetrahedron can be constructed. For example, at large values of $\bar{\sigma}$, $V^2$ becomes negative when $\eta\neq 0$:

$$144\,V^2\rightarrow\begin{cases}-\bar{\sigma}^4 & \text{when } \eta\neq 0\\ [(k+\frac{1}{2})^2-\tau^2][(j_t+\frac{1}{2})^2-1]\bar{\sigma}^2 & \text{when } \eta=0\end{cases}. \tag{11}$$

A negative value of the square volume is viewed as analogous to a negative value of the squared momentum of a particle in a classically forbidden region. In this view the squared volume of the tetrahedron plays the role of the kinetic energy of an angular motion and Ponzano and Regge develop a semiclassical expression of $6j$ coefficients analogous to a WKB wave function. The Ponzano-Regge formula, based on an earlier one by Wigner,[8] is

$$\begin{Bmatrix}abc\\ def\end{Bmatrix}\approx\begin{cases}\dfrac{1}{\sqrt{12\pi V}}\cos\left[\sum\limits_{h>k=1}^{4}j_{hk}\theta_{hk}+\frac{1}{4}\pi\right] & \text{when } V^2>0\\ \dfrac{1}{2\sqrt{12\pi\,|V|}}\cos\Phi\exp\left[-\left|\sum\limits_{\substack{h>k\\ h,k}}j_{hk}\mathrm{Im}\theta_{hk}\right|\right] & \text{when } V^2<0\end{cases}, \tag{12}$$

where

$$\Phi=\sum_{\substack{h>k\\ h,k}}(j_{hk}-\tfrac{1}{2})\mathrm{Re}\theta_{hk}, \tag{13}$$

and $\theta_{hk}$ is the angle between the outer-normals of the tetrahedron faces that intersect along $j_{hk}$, generally complex for $V^2<0$. The occurrence of a classically forbidden range is illustrated by considering the case of $(a,b,c,d,e)\gg(f,|e-a|,|d-b|)$, studied by Edmonds,[9] and by Brussaard and Tolhoek,[10] where the $6j$ coefficient reduces to the rotational matrix $d^{(f)}_{d-b,e-a}(\theta)$, an eigenfunction of the symmetric top. Regions near the poles of $\theta$ are classically forbidden by the centrifugal potential of the azimuthal motion when $(d-b,e-a)\neq 0$.

The result obtained in Sec. II implies that *$\eta=0$ processes are classically favored and $\zeta=0$ processes are classically unfavored.* Note that for $\eta=0$, both angular momenta of the projectile increase or decrease [i.e., $(l_a,l'_a)\gtrless(l_b,l'_b)$] whereas for $\zeta=0$ either $(l_a>l_b,l'_a<l'_b)$ or $(l_a<l_b,l'_a>l'_b)$.

Section II may have implied that the value of the $6j$ coefficient is much smaller in the classically forbidden range than in the allowed range, while the phase factor $\cos\Omega$ in (12) oscillates between positive and negative values, probably causing extensive cancellations in the cross section and orientation formulas. The following analysis of the values of $6j$ coefficients as functions of the symmetrical quantum numbers does not bear out these surmises. Parity conservation will be shown to play an important role for this.

When $\eta=0$, and $\bar{\sigma}\gg 1$, the limiting values of $\theta_{hk}$ in (12) are $\theta_{12}=\theta_{34}\rightarrow\pi$ and $\theta_{13}=\theta_{14}=\theta_{24}=\theta_{23}\rightarrow\pi/2$, whereby $\sum j_{hk}\theta_{hk}\rightarrow(\bar{\sigma}+k+j_t+1)\pi$. Parity restricts $\bar{\sigma}+k$ to even values, whereby $\cos(\sum j_{hk}\theta_{hk}+\pi/4)\rightarrow\cos(\pi/4)=1/\sqrt{2}$ regardless of any value of $\tau$ and $k$. This value coincides with the root mean square of the cosine and therefore with the result of Wigner's classical vector model. A numerical study shows that the Airy function representation, which replaces (12) near the classical turning point, approximates the values of the $6j$ coefficient very well at large values of $\bar{\sigma}$, for reasons that remain unclear. If a $6j$ coefficient lies close to a classical turning point, then its phase $\Omega=\sum j_{hk}\theta_{hk}+\pi/4$ measured from a turning point is given by[6] $|\Omega-\Omega_{V^2}|\approx 9|V^3|/2\prod_{h=1}^{4}A_h$ which goes to zero for

TABLE I. The values of $6j$ coefficients when $\zeta=0$ and classically forbidden and when $\eta=0$ and classically allowed.

| $k$ | $\tau$ | $\zeta$ | $\eta$ | $\bar{\sigma}$ | $6j$ |
|---|---|---|---|---|---|
| 1 | 0 | 0 | 1 | 4 | 0.3333[−01] |
| | | | | 6 | 0.9524[−02] |
| | | | | 8 | 0.3968[−02] |
| | | | | 10 | 0.2020[−02] |
| | | | | 12 | 0.1166[−02] |
| | | | | 14 | 0.7326[−03] |
| | | | | 16 | 0.4902[−03] |
| | | | | 18 | 0.3440[−03] |
| | | | | 20 | 0.2506[−03] |
| | | | | 22 | 0.1882[−03] |
| 1 | 1 | 1 | 0 | 3 | 0.3333 |
| | | | | 5 | 0.2000 |
| | | | | 7 | 0.1429 |
| | | | | 9 | 0.1111 |
| | | | | 11 | 0.9091[−01] |
| | | | | 13 | 0.7692[−01] |
| | | | | 15 | 0.6667[−01] |
| | | | | 17 | 0.5882[−01] |
| | | | | 19 | 0.5263[−01] |

$\eta=0$ as $\bar{\sigma}$ increases. But note that this is a necessary condition for a $6j$ coefficient to lie close to a turning point, not a sufficient one. The amplitude factor $1/\sqrt{12\pi V}$ of (12) approaches $\bar{\sigma}^{-1}\{\pi[(k+\frac{1}{2})^2-\tau^2][(j_t+\frac{1}{2})^2-1]\}^{-1/2}$ [Eq. (11)] as $\bar{\sigma}$ becomes large, i.e., the $6j$ coefficients vary inversely to $\bar{\sigma}$ and $k$ for $(\bar{\sigma},k)\gg 1$, and to $[(k+\frac{1}{2})^2-\tau^2]^{-1/2}$ as functions of $\tau$. The larger is $\tau$, i.e., the thinner is the tetrahedron, the larger is the $6j$ coefficient.

When $\zeta=0$, at large values of $\bar{\sigma}$, $\mathrm{Re}\theta_{12}=\mathrm{Re}\theta_{34}\to\pi$, $\mathrm{Re}\theta_{13}=\mathrm{Re}\theta_{24}\to 0$ $(\pi)$ and $\mathrm{Re}\theta_{14}=\mathrm{Re}\theta_{23}\to\pi$ (0) for $\eta=1$ $(\eta=-1)$, resulting in $\cos\Phi=\cos[(\bar{\sigma}\pm\eta+j_t+k)\pi]$ which is 1 again due to parity. $\mathrm{Im}\theta_{12}$ and $\mathrm{Im}\theta_{34}$ approach a constant value but

$$\eta\mathrm{Im}\theta_{13}=-\eta\mathrm{Im}\theta_{14}=\eta\mathrm{Im}\theta_{24}=-\eta\mathrm{Im}\theta_{23}\to\ln\bar{\sigma}$$

and

$$\exp\left[-\left|\sum j_{hk}\mathrm{Im}\theta_{hk}\right|\right]\to\exp(-2\ln\bar{\sigma})$$

which becomes much smaller than $1/\sqrt{2}$ as $\bar{\sigma}$ increases. A numerical study shows that the value (12) approximates the $6j$ coefficient very well, meaning that it lies far from the classical turning point at large values of $\bar{\sigma}$. The phase measured from the turning point, in this case, goes to infinity as $\bar{\sigma}$ increases, as expected. The amplitude factor of (12) varies inversely to the square of $\bar{\sigma}$, decreasing faster by one power for $\zeta=0$ than for $\eta=0$. Therefore the magnitude of the $6j$ coefficient is quite different at large $\bar{\sigma}$ for $\eta=0$ and $\zeta=0$, in contrast to its variation in $\bar{\sigma},\tau$, and $k$.

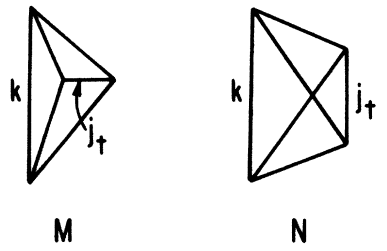


FIG. 5. The tetrahedron collapsed into the plane diagrams $M$ and $N$ corresponding to $\eta=0$ and $\zeta=0$, respectively, for $V^2=0$. The topological difference between $M$ and $N$ disappears as soon as $V^2$ takes nonzero values.

At small values of $\bar{\sigma}$, the angles $\theta_{hk}$ of the tetrahedron in (12) do not differ greatly from their values for $V^2=0$ (for the physically significant range of $k$ as discussed in Secs. II A and II B). When $V^2=0$, the tetrahedron collapses into a plane, and is represented by two topologically different diagrams $M$ and $N$ in Fig. 5, depending on whether the fourth vertex lies inside ($M$) or outside ($N$) the triangle composed of three other vertices. Diagram $M$ corresponds to $\eta=0$ since two hyperbolas coincide in Fig. 4 and $N$ to $\zeta=0$ as seen in Fig. 3.

When $\eta=0$, the tetrahedron shape elongates from diagram $M$, as $\bar{\sigma}$ increases, without major distortion. The phase $\Omega=\sum j_{hk}\theta_{hk}+\pi/4$ amounts to $(k+\bar{\sigma}\pm\zeta)\pi+7\pi/4$ for diagram $M$ (at $V^2=0$) so that $\cos\Omega=1/\sqrt{2}$, as it does at large values of $\bar{\sigma}$ since $\bar{\sigma}+k$ is even. The change of the phase as a function of $\bar{\sigma}$ is given by $\partial\Omega/\partial\bar{\sigma}=(\theta_{13}+\theta_{14}+\theta_{24}+\theta_{23})/2$ which equals $\pi$ regardless of $k$ both for diagram $M$ and for large $\bar{\sigma}$. But the value of $\cos\Omega$ remains close to $1/\sqrt{2}$ with same sign regardless of $k$ and $\tau$ for both small and large values of $\bar{\sigma}$ because $\bar{\sigma}$ changes in steps of 2. Therefore, $\cos\Omega$ is expected to remain close to $1/\sqrt{2}$ over the whole range of $\bar{\sigma}$.

When $\zeta=0$, as we saw in Sec. II A, the tetrahedron belongs to a classically allowed range for only a few values of $\bar{\sigma}$, where it takes an $N$-like shape with $6j$ values comparable to those for $\eta=0$. Except for these few cases, the magnitude of the $6j$ coefficients is much larger for $\eta=0$ than for $\zeta=0$ and remains uniform in its sign and magnitude as shown in Table I.

## IV. DISCUSSION

Our discussion of the classically forbidden and allowed ranges in the framework of the symmetrical quantum numbers pertains to the system (1) and rests on the formula[11]

$$\begin{Bmatrix} l_a & l_b & j_t \\ l_a' & l_b' & j_t \\ k & k & 1 \end{Bmatrix}=(-1)^{l_a'+l_b+k+j_t}\frac{[l_a(l_a+1)-l_b(l_b+1)-l_a'(l_a'+1)+l_b'(l_b'+1)]}{2[k(k+1)(2k+1)j_t(j_t+1)(2j_t+1)]^{1/2}}\begin{Bmatrix} l_a & l_b & j_t \\ l_b' & l_a' & k \end{Bmatrix}. \tag{14}$$

The $6j$ coefficient appearing on the right-hand side of (14) implies the vector relations (2) and (3), more restrictive than would be implied by the $9j$ coefficient on the left-hand side. The special case (14) allows $[l_a(l_a+1)-l_b(l_b+1)-l'_a(l'_a+1)+l'_b(l'_b+1)]/2$ to be interpreted as $\mathbf{j}_t\cdot\mathbf{k}$ (Appendix A). This does not mean that vector relations (2) and (3) are true physical relations. The classically forbidden and allowed properties, though discussed under this assumption, can be accepted as real since this property has direct consequences on the magnitudes of $9j$ coefficients. The general case of a $9j$ coefficient

$$\begin{Bmatrix} l_a & l_b & j_t \\ l'_a & l'_b & j'_t \\ k_a & k_b & K \end{Bmatrix}$$

with $j_t\neq j'_t$ and/or $k_a\neq k_b$ and/or $K\neq 1$ remains to be studied.


## ACKNOWLEDGMENT

I would like to thank Professor U. Fano for his encouragement, guidance, and support. His contributions to both the substance and structure of this manuscript are greatly acknowledged. This work was supported by the U.S. Department of Energy (Office of Basic Science).


## APPENDIX A

Here let us derive the following relation:

$$\mathbf{j}_t\cdot\mathbf{k}=\tfrac{1}{2}[\,l_a(l_a+1)-l_b(l_b+1)-l'_a(l'_a+1)+l'_b(l'_b+1)]\,. \tag{A1}$$

Let the coordinates of $\mathbf{F},\mathbf{A},\mathbf{B},\mathbf{F}'$ of Fig. 2 be (0,0,0), $(x_1,x_2,x_3)$, $(y_1,y_2,y_3)$, and $(z_1,z_2,z_3)$, respectively. Then we have

$$\begin{aligned}&(\mathbf{A}-\mathbf{F})^2=\sum_i x_i^2,\quad (\mathbf{B}-\mathbf{F})^2=\sum_i y_i^2\,,\\ &(\mathbf{A}-\mathbf{F}')^2=\sum_i (x_i-z_i)^2,\quad (\mathbf{F}-\mathbf{F}')^2=\sum_i z_i^2\,,\\ &(\mathbf{B}-\mathbf{F}')^2=\sum_i (y_i-z_i)^2\,.\end{aligned} \tag{A2}$$

The scalar product of $\mathbf{j}_t$ and $\mathbf{k}$ can be expressed with the above quantities:

$$\begin{aligned}\mathbf{j}_t\cdot\mathbf{k}&=\sum_i (x_i-y_i)z_i\\ &=-\tfrac{1}{2}[(\mathbf{A}-\mathbf{F}')^2-(\mathbf{A}-\mathbf{F})^2-(\mathbf{F}-\mathbf{F}')^2]\\ &\quad+\tfrac{1}{2}[(\mathbf{B}-\mathbf{F}')^2-(\mathbf{B}-\mathbf{F})^2-(\mathbf{F}-\mathbf{F}')^2]\\ &=\tfrac{1}{2}[(l_a+\tfrac{1}{2})^2-(l_b+\tfrac{1}{2})^2-(l'_a+\tfrac{1}{2})^2+(l'_b+\tfrac{1}{2})^2]\,.\end{aligned} \tag{A3}$$

In terms of symmetrical quantum numbers

$$\mathbf{j}_t\cdot\mathbf{k}=\begin{cases}\tau\zeta, & \eta=0\\ \bar{\sigma}\eta, & \eta\neq 0\,.\end{cases} \tag{A4}$$

For $\eta\neq 0$, $\hat{\mathbf{j}}_t\cdot\hat{\mathbf{k}}$ can be larger than unity because of the reason considered in Secs. II and III. Notice that the value of $\bar{\sigma}$ from which $\hat{\mathbf{j}}_t\cdot\hat{\mathbf{k}}$ becomes larger than unity does not depend on that of $\tau$ for $\eta\neq 0$.


[1] U. Fano and J. Macek, Rev. Mod. Phys. **45**, 553 (1973).

[2] F. Blatt and L. C. Biedenharn, Rev. Mod. Phys. **25**, 258 (1953).

[3] C. W. Lee and U. Fano, Phys. Rev. A **33**, 921 (1986).

[4] M. Kohmoto and U. Fano, J. Phys. B **14**, L447 (1981).

[5] J. Schwinger, in *Quantum Theory of Angular Momentum*, edited by L. C. Biedenharn and H. Van Dam (Academic, New York, 1965), p. 259.

[6] G. Ponzano and T. Regge, in *Spectroscopic and Group Theoretical Methods in Physics*, edited by F. Bloch *et al.* (North Holland, Amsterdam, 1968), p. 1.

[7] L. C. Biedenharn and J. D. Louck, *The Racah-Wigner Algebra in Quantum Theory, Encyclopedia of Mathematics and Its Applications, Vol. 9* (Addison-Wesley, Reading, Mass., 1981), p. 369.

[8] E. P. Wigner, *Group Theory and Its Application to the Quantum Mechanics of Atomic Spectra* (Academic, New York, 1959), p. 353.

[9] A. Edmonds, *Angular Momentum in Quantum Mechanics* (Princeton, New Jersey, 1957), p. 122.

[10] P. J. Brussard and H. A. Tolhoek, Physica **23**, 955 (1957).

[11] M. Rotenberg *et al.*, *The 3j and 6j Symbols* (MIT, Cambridge, 1959).